Spiking Neural Network With Distributed Plasticity Reproduces Cerebellar Learning in Eye Blink Conditioning Paradigms

Alberto Antonietti*, Claudia Casellato, Jesús A. Garrido, Niceto R. Luque, Francisco Naveros, Eduardo Ros, Egidio D'Angelo, and Alessandra Pedrocchi

Abstract—*Goal:* In this study, we defined a realistic cerebellar model through the use of artificial spiking neural networks, testing it in computational simulations that reproduce associative motor tasks in multiple sessions of acquisition and extinction. *Methods:* By evolutionary algorithms, we tuned the cerebellar microcircuit to find out the near-optimal plasticity mechanism parameters that better reproduced human-like behavior in eye blink classical conditioning, one of the most extensively studied paradigms related to the cerebellum. We used two models: one with only the cortical plasticity and another including two additional plasticity sites at nuclear level. *Results:* First, both spiking cerebellar models were able to well reproduce the real human behaviors, in terms of both "timing" and "amplitude", expressing rapid acquisition, stable late acquisition, rapid extinction, and faster reacquisition of an associative motor task. Even though the model with only the cortical plasticity site showed good learning capabilities, the model with distributed plasticity produced faster and more stable acquisition of conditioned responses in the reacquisition phase. This behavior is explained by the effect of the nuclear plasticities, which have slow dynamics and can express memory consolidation and saving. *Conclusions:* We showed how the spiking dynamics of multiple interactive neural mechanisms implicitly drive multiple essential components of complex learning processes. *Significance:* This study presents a very advanced computational model, developed together by biomedical engineers, computer scientists, and neuroscientists. Since its realistic features, the proposed model can provide confirmations and suggestions about neurophysiological and pathological hypotheses and can be used in challenging clinical applications.

Index Terms—Artificial spiking neural network, cerebellum, distributed plasticity, genetic algorithm (GA), model tuning, motor learning, Pavlovian conditioning.

*A. Antonietti is with the NeuroEngineering and Medical Robotics Laboratory, Department of Electronics, Information and Bioengineering, Politecnico di Milano, Piazza Leonardo da Vinci 32, 20133, Milano, Italy (e-mail: alberto.antonietti@polimi.it).

C. Casellato and A. Pedrocchi are with the NeuroEngineering and Medical Robotics Laboratory, Department of Electronics, Information and Bioengineering, Politecnico di Milano.

J. A. Garrido, N. R. Luque, F. Naveros, and E. Ros are with the Department of Computer Architecture and Technology, University of Granada.

E. D'Angelo is with the Brain Connectivity Center, IRCCS Istituto Neurologico Nazionale C. Mondino and the Department of Brain and Behavioral Sciences, University of Pavia.

I. INTRODUCTION

THE cerebellum is a fundamental processing unit for a large number of cognitive and motor tasks [1]. One of the most studied paradigms of cerebellum involvement is the eye blink classical conditioning (EBCC) [2]. In the standard EBCC, a neutral conditioned stimulus (CS), e.g., a tone, precedes an attentive unconditioned stimulus (US), e.g., an air-puff directed to the eye. The time interval between the onset of the CS and the onset of US, i.e., the interstimulus interval (ISI), is kept constant during the session trials [3]. At the beginning, the (animal or human) subjects show eyelid closures (blink) elicited by the US. After repeated presentations of CS and US paired during the acquisition phase, the subject learns to blink before the US arrival; this action is called conditioned response (CR). During the extinction phase, the subject continues to receive the CS only, but without the presentation of US. At the beginning, the learned association still leads to generate CRs. However, the unneeded anticipated blink response is rapidly extinguished.

Several studies proved the importance of the cerebellum for the acquisition and extinction of CRs in EBCC sessions. The signal pathways involved during the EBCC have been established in the literature [see Fig. 1(a)]. The CS is conveyed from the Pontine Nuclei to the Granular Cells (GRs) through the Mossy Fibers (MFs) [4]. On the other hand, the US is conveyed from the Inferior Olive Cells (IOs) to the Purkinje Cells (PCs) through the Climbing Fibers (CFs) [5]. The PCs also receive excitatory synapses from GRs through the parallel fibers (PFs). Finally, the eyelid closure is commanded by the deep cerebellar nuclei (DCNs), which excite the related motor neurons.

The learning capabilities of the cerebellum are related to the plasticity mechanisms that change the synaptic weights of the connections between different groups of cells [6]–[8]. There are two well-known long-term plasticities for the PF-PC connections: long term potentiation (LTP) and long term depression (LTD). They are assumed to be responsible for the CR acquisition and extinction [9]. In the last years, other plasticity sites have been hypothesized [10]–[14], both at cortical and nuclear levels [15]–[17], in order to take into account the different time scales which can be identified in cerebellar adaptation. More specifically, the cerebellar learning can be separated into two components: a fast process related to the cortical plasticity and a slow process associated to the nuclear plasticity.

The simplicity of the EBCC and the timing nature of the protocol have led to the use of this paradigm as a test bench for computational models of the cerebellum, which range from
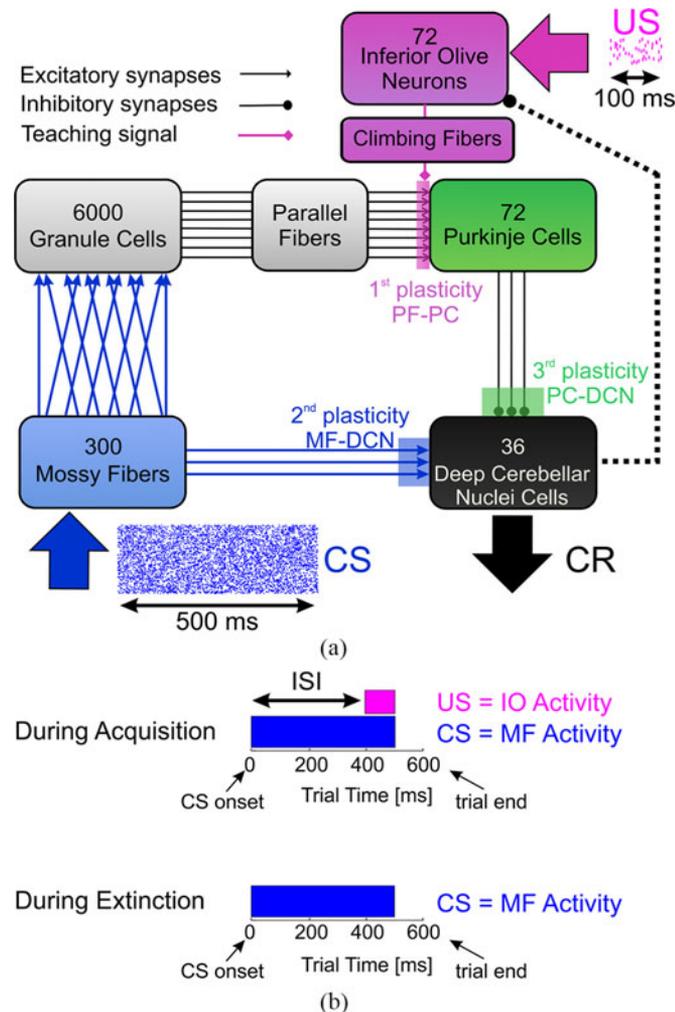
Fig. 1. (a) SNN topology, with connections between the specific cell populations, and the input and output signals for EBCC simulations. The model was equipped with three plasticity sites, each bidirectional (LTP and LTD), indicated by the transparent areas: PF–PC (pink), MF-DCN (blue), and PC-DCN (green). For the 1–plasticity model, only the first plasticity was active. For the 3–plasticity model, also the second and third plasticities were enabled. The inhibitory connection from DCN to IO is dashed because it was implemented as an external inhibitory mechanism. (b) EBCC protocol scheme. During the acquisition trials, pairs of CS and US were presented as spike patterns to the cerebellar microcircuit, at a predefined ISI. The SNN learned to generate CR. During extinction trials, the only input to the SNN was the CS.

simplified analog versions [18]–[20] to more realistic models using artificial spiking neural networks (SNN) [21], [22]. The majority of the published models has only taken into account the cortical plasticity. A recent example is the large–scale SNN (more than 100 thousands of neurons) developed by Yamazaki and Igarashi used during a robotic Pavlovian task to reproduce the learning mechanisms by PF-PC plasticity [22]. Additionally, Casellato *et al.* have embedded and tested a SNN-based cerebellar model during different tasks, such as EBCC and vestibuloocular reflex, both in computational simulations and in real-robotic platforms [23]. This model has shown its effectiveness obtaining behaviors similar to neurophysiological experiments, exploiting only LTP and LTD plasticities at the PF-PC connections.

This study aims at improving the latter SNN model, testing two additional plasticities at the nuclear level: LTP and LTD

mechanisms at MF-DCN and PC-DCN synapses. We embedded the models in closed-loop computational simulations reproducing the EBCC protocol with two sessions, each comprised of an acquisition and an extinction phases.

Whereas the inclusion of realistic plasticity equations, spiking neural dynamics, and recurrent topologies enhanced the descriptive power of SNNs, it also increased the number of free parameters, hence requiring an efficient and automated tuning [24]. In particular, we exploited metaheuristic techniques (evolutionary algorithms) to obtain the cerebellar–model plasticity parameters that better reproduced the physiological behaviors observed in humans. Even if a complete theoretical basis is not available yet, metaheuristic methods for optimization are widely used to find solutions to problems where the search space is complex [25].

Our aim is to highlight the behavioral outcomes produced by the cerebellar multiple dynamics and, by comparing the SNN model equipped with only the cortical plasticity and the model with three plasticity sites, to confer specific roles on the plasticity mechanisms.

II. MATERIALS AND METHODS

A. Cerebellar Model

We started from a well-tested cerebellar model, exploiting the event-driven simulator based on look-up-tables [26], an open-source simulator of SNN (available online at http://code. google.com/p/edlut/) that speeds up the simulation through the use of look-up tables; thus, reducing the computational load. All the experiments were performed on a desktop PC (Intel Core i7-2600 CPU at 3.40 GHz).

The SNN (see Fig. 1(a)] was composed of 6480 leaky integrateand-fire neurons that replicated the cerebellar topology: 300 MFs, which were excited by the CS; 6000 GRs; 72 IOs, which received the US; 72 PCs; 36 DCNs, which produced the cerebellar output and, therefore, the CRs.

The MFs were randomly connected with the GRs, and each GR received four random connections, for a total of 24 000 excitatory synapses. The granular layer was a sparse representation of the state of the system encoded by the MFs, with each time sample (1 ms) corresponding to a nonrecurrent state of this layer. The largest number of synapses involved the PFs, since they randomly linked each PC with the 80 of the GRs, for a total of 345444 connections. The 72 CFs constituted one–to–one teaching connections between IOs and PCs. Each DCN received excitatory synapses from all the 300 MFs (10 800 synapses in total) and inhibitory connections from two PCs (72 synapses in total). Since the harmfulness of the US diminishes when the eyelid closure protects the cornea, we implemented a DCN-IO inhibitory loop. This mechanism halved the incoming US-related IOs firing rate when a CR was generated just before the US onset. The nucleoolivary inhibitory loop translated the motor command signal into a sensory modulation; thus, a single cerebellar area simultaneously tackled both motor execution and sensory prediction [27].

1) Learning Rules: The 3–plasticity and 1–plasticity SNN computational models were tested, to compare the learning properties of cerebellum models that go beyond the classic

PF-PC adaptive mechanism. The 3-plasticity model embedded three plasticity sites (PF-PC, MF–DCN, and PC–DCN), whereas the 1–plasticity model embedded only the cortical plasticity (PF-PC).

The synaptic weights of each plasticity site evolved following three different learning rules.

a) First learning rule: PF-PC:

$$W_{\mathrm{PF}_i \mathrm{PC}_j}(t) =$$

$$\begin{cases} \beta_1 \int\limits_{-\infty}^{\mathrm{IO\,spike}_j} K(t-x)\,\delta_{PF_i}(t-x)\,dx, & \text{if } PC_i \text{ active} \\ & \text{and } t = t_{\mathrm{IO\,spike}_j} \\ \alpha_1, & \text{if } PC_i \text{ active} \\ & \text{and } t \neq t_{\mathrm{IO\,spike}_j} \\ 0, & \text{otherwise} \end{cases}$$

$$(1)$$

where

$$\delta_{PF_i}(s) = \begin{cases} 1, & \text{if } PF_i \text{ is active at time } s \\ 0, & \text{otherwise} \end{cases} \quad (2)$$

and the Kernel function is

$$K(z) = A \cdot e^{\frac{-z-t_0}{\tau}} \left(\sin\left(2\pi \frac{z-t_0}{\tau}\right) \right)^{20} \quad (3)$$

where β_1 is the LTD$_1$ constant; α_1 is the LTP$_1$ constant; $t_{\mathrm{IO\,spike}j}$ is the time when the corresponding CF$_j$ emitted a spike; K is the integral kernel function, which had its peak at t_0 before $t_{\mathrm{IO\,spike}j}$. t_0 was set to 100 ms, matching the physiological delay of the neural circuit dictated by biology [28]. τ and A are constant factors to normalize the kernel. More detailed explanations about the rationale of the kernel function can be found in [26].

b) Second learning rule: MF-DCN:

$$W_{\mathrm{MF}_i-\mathrm{DCN}_j}(t) =$$

$$\begin{cases} \beta_2 \int\limits_{-\infty}^{+\infty} K(t-x)\,\delta_{\mathrm{MF}_i}(t-x)\,dx, & \text{if } \mathrm{MF}_i \text{ active} \\ & t = t_{\mathrm{PC\,spike}_j} \\ \alpha_2, & \text{if } \mathrm{MF}_i \text{ active} \\ & t \neq t_{\mathrm{PC\,spike}_j} \\ 0, & \text{otherwise} \end{cases}$$

$$(4)$$

where

$$\delta_{\mathrm{MF}_i}(s) = \begin{cases} 1, & \text{if } \mathrm{MF}_i \text{ is active at time } s \\ 0, & \text{otherwise} \end{cases} \quad (5)$$

and the Kernel function is

$$K(z) = e^{-\frac{|z|}{\tau}} \left(\cos\left(\frac{z}{\tau}\right) \right)^2 \quad (6)$$

where β_2 is the LTD$_2$ constant, α_2 is the LTP$_2$ constant; $t_{\mathrm{PC\,spike}j}$ is the time when one of the two corresponding PC_j emitted a spike; K is the integral Kernel function, and τ is a normalization factor for the arguments in the learning rule.

c) Third learning rule: PC-DCN: The third learning rule corresponds to a classic spike-timing-dependent plasticity. When a PCs spike was immediately followed (within an LTP–time

window set to 20 ms) by the spike of the corresponding DCN, the inhibitory synapses from the two PCs to that DCN were increased. This strengthening (maximum LTP change defined by LTP$_3$ constant) depended on the delay between PC and DCN spikes. Otherwise, if the opposite chronological order occurred (within an LTD-time window set to 60 ms), the synapses underwent LTD (maximum LTD change defined by LTD$_3$ constant).

The six LTP and LTD constants (LTP$_1$, LTD$_1$, LTP$_2$, LTD$_2$, LTP$_3$, and LTD$_3$) for the three learning rules were defined using a metaheuristic parameter optimization as explained in Section II-C.

B. Protocol

We used the "delayed EBCC" protocol [CS and US coterminate, see Fig. 1(b)] in order to test the models' capability to acquire and extinguish CRs. The protocol was divided in two sessions of 100 trials (session$_1$ and session$_2$); each session was composed of an acquisition phase, with the presentation of CS-US pairs during 80 trials (acquisition$_1$ and acquisition$_2$), and an extinction phase, with the presentation of only CS for 20 trials (extinction$_1$ and extinction$_2$). We set the ISI equal to 400 ms, which is a standard value used in EBCC studies [3], [29], [30]. The CS lasted 500 ms, equal to the ISI plus the duration of US (100 ms). Between two consecutive trials, we inserted a pause of 100 ms, during which the network was silent.

We also tested the robustness of the models when increasing and decreasing the ISI (350 and 450 ms).

During the CS, the firing rate of MFs varied within a random uniform distribution between 40 and 50 Hz. During the US, IOs fired with a mean firing rate of 1 Hz and maximum firing rate of 10 Hz [31]. The DCNs spiking activity was decoded into the "cerebellar output" variable using a firing rate approach [21]. A CR was identified when the cerebellar output variable overcame a predefined threshold equal to 50. When a CR was identified, the IOs activity during the following US was reduced by 50%, due to the DCN-IO inhibitory loop.

C. Cerebellar Model Tuning

The tuning consisted on the regulation of 9 variables: the LTP and LTD constants and the initialization weights of the plastic synapses, for the three learning rules (LTP$_1$, LTD$_1$, w_{0_1} LTP$_2$, LTD$_2$, w_{0_2}, LTP$_3$, LTD$_3$, and w_{0_3}). Whereas previous works used a trial–and–error approach [32], [33], in this study, we adopted a genetic algorithm (GA) to tune the 3–plasticity model parameters. The GA was written in MATLAB language, which automatically triggered each simulation, carrying out EBCC sessions driven by the model equipped with the updated genes. Each generation was composed of 12 individuals, each identified by the nine genes. For each individual, a complete EBCC simulation was carried out. The range of each gene was established using admissible values found in the literature; for the LTP and LTD constants, we referred to works based on similar architectures [20], [21], [23], [32], [34] and neurophysiological restrictions (e.g., LTP$_1$ lower than LTD$_1$ and LTP-LTD$_{2,3}$ constants lower than LTP-LTD$_1$). The three initial weights (genes 3, 6, and 9) could vary between the 10% and the 90% of the whole range in which the weights of those plastic connections

TABLE I
GENES AND THEIR UPPER AND LOWER BOUNDS

PF-PC	LTP_1	LTD_1	w_{0_1} [nS]
Upper Bound	0.05	-10^{-10}	0.2
Lower Bound	10^{-10}	-1.5	1.8
MF-DCN	LTP_2	LTD_2	w_{0_2} [nS]
Upper Bound	10^{-6}	-10^{-10}	0.0035
Lower Bound	10^{-10}	-10^{-7}	0.0315
PC-DCN	LTP_3	LTD_3	w_{0_3} [nS]
Upper Bound	10^{-6}	10^{-7}	0.15
Lower Bound	10^{-10}	10^{-10}	1.35

could move during the learning protocols. This way, both LTP and LTD could occur with respect to the initial "naïve" network state. The possible values assumed by the plastic weights during the simulation were set to enclose the firing rate of the different groups of cells within neurophysiological values [35]. The upper and lower bounds for each gene are reported in Table I.

The key element of a correct tuning using a GA is the fitness function, which allows the evaluation of the suitability of each individual, according to the specific aims. In our case, the fitness function was designed to obtain a physiological outcome, i.e., the percentage of CRs across the trials, during the four phases of the protocol (acquisition$_1$, extinction$_1$, acquisition$_2$, and extinction$_2$). We considered two components: the capability to reach a certain CR% during the acquisition phases, and the capability to rapidly extinguish the previously acquired behavior. We designed the fitness function (7), ranging from zero to one, to be maximized in order to obtain a behavioral outcome similar to human data

$$\text{fitness} = \text{fit}_{\text{acq1}} \cdot \text{fit}_{\text{ext1}} \cdot \text{fit}_{\text{acq2}} \cdot \text{fit}_{\text{ext2}} \cdot \text{saturation} \quad (7)$$

where fit_{acq1} and fit_{acq2} were the same function (8), applied to acquisition$_1$ and acquisition$_2$, respectively. fit_{ext1} and fit_{ext2} also represented the same function (10) applied to extinction$_1$ and extinction$_2$, respectively. The function saturation (12) operated overall as a penalty if the CRs number was "unphysiologically" saturated at 100%

$$\text{fit}_{\text{acq}} = \begin{cases} 1, & \text{if } n_{\text{acq}} \le 50 \\ 1 - \left(\frac{n_{\text{acq}}-50}{30}\right)^3 \cdot 0.95, & \text{if } 50 < n_{\text{acq}} \le 80 \\ 0, & \text{if } n_{\text{acq}} > 80 \end{cases} \quad (8)$$

where

$$n_{\text{acq}} = \min(81, N)$$
$$N|\text{CR}\%(N) \ge 70\% \cup \text{CR}\%(N \ge \forall \text{trial} \ge 80) \ge 60\%. \quad (9)$$

The optimal CR% had to reach a value of 70% and remain firmly above 60%, before the 50th trial (N) of acquisition. If the conditions imposed in (9) were satisfied for $N > 50$, the function value exponentially decreased toward its minimum value (0.05). If the conditions were not satisfied before the last trial of

acquisition (80th), the function value was set to zero

$$\text{fit}_{\text{ext}} = \begin{cases} 0.19 \cdot n_{\text{ext}} + 0.05, & \text{if } n_{\text{ext}} < 5 \\ 1, & \text{if } 5 \le n_{\text{ext}} \le 10 \\ 1 - \left(\frac{n_{ext}-10}{10}\right)^3 \cdot 0.95, & \text{if } 10 < n_{\text{ext}} \le 20 \\ 0, & \text{if } n_{\text{ext}} > 20 \end{cases} \quad (10)$$

where

$$n_{\text{ext}} = \min(21, N)$$
$$N|\text{CR}\%(N) \le 20\%$$
$$\cup \text{CR}\%(N \ge \forall \text{trial} \ge 20) \le 20\%. \quad (11)$$

The optimal CR% had to decrease under a value of 20% between the fifth and the tenth trial of extinction. If the threshold was crossed too early or too late, the function value decreased toward its minimum value (0.05) with a linear or exponential trend, respectively. If the threshold was not crossed, the condition set by (11) was not satisfied, and the function value was set zero

$$\text{saturation} = \begin{cases} 1, & \text{if } N\text{sat} \le 20 \\ 1 - \frac{N\text{sat}}{200}, & \text{otherwise} \end{cases} \quad (12)$$

where Nsat is the number of trials where CR% is equal to 100%. This term linearly decreased the fitness value if the number of "saturated" trials was greater than 20.

The algorithm to define the 12 individuals of the following generation took into account selection, crossover, and mutation. The four individuals with the best fitness of their generation were kept as they were, whereas the other eight individuals were generated by means of the following steps. The *roulette wheel* process selected the potential parents of the following generation, applying a probability proportional to their fitness [36]. Then, among these eight individuals, there was an 80% of probability to perform a crossover between two parents: the uniform crossover swapped four randomly selected genes between the two parents. After the crossover process, each individual had a probability of 90% to go through a mutation: a uniform random reextraction from the gene range of definition (see Table I) for individuals 5–8 or a Gaussian mutation starting from genes' current values. After these steps, the final 12 individuals of the following generation were defined and the new 12 EBCC simulations started. If the increasing of the maximum fitness value between two successive generations was lower than 0.1% for 100 consecutive generations, the GA terminated and the near–optimal model parameters were found out.

D. Data Analysis

For the whole analysis, we tested the data normality with the Anderson–Darling test, in order to choose the proper statistical tests. Nonnormally distributed variables were indicated as "median [25th percentile 75th percentile]."

The results of the GA optimization were evaluated considering all the individuals with the optimal fitness values (i.e., fitness equal to one). When more than one individual matched this criterion, the robustness of the results was preserved
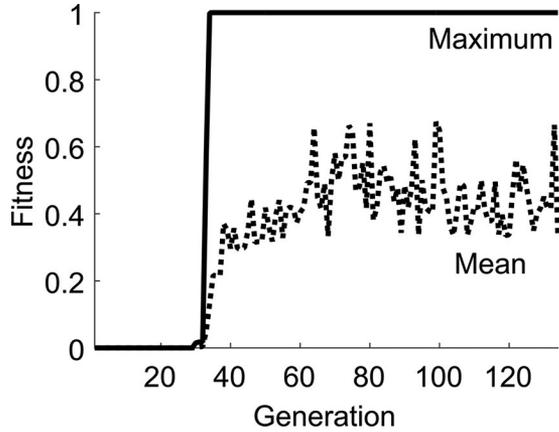
Fig. 2.   GA: Fitness values along generations. The dashed line represents the mean fitness values across the 12 individuals for each generation, whereas the maximum value is plotted as a solid line.

by considering multiple good solutions that guaranteed the characteristics of the CR acquisition and extinction; thus, we obtained a population of near-optimal 3–plasticity models.

As expected, due to the elitism of the GA, the maximum fitness values monotonically increased along the generations (see Fig. 2). The GA stopped after 133 generations, testing 1596 combinations (individuals) of the nine genes. Among them, 109 individuals had fitness values equal to one and they constituted the 3–plasticity model population. The same 109 individuals were modified, blocking the MF-DCN and PC–DCN plasticity sites (i.e., setting to zero genes 4–5 and 7–8, i.e. LTP_2, LTD_2, LTP_3, and LTD_3). They constituted the 1–plasticity model population that was compared to the 3–plasticity one.

For each of the two model populations, we measured the percentage of CRs along the whole simulation, with a moving window of ten trials, and the latency of CRs, defined as the time difference between the CR and US onsets. For both populations, we computed:

1) The median and interquartile ranges of the trial number when the threshold of 70% was reached by the CR%;
2) the median and interquartile ranges of the CR% in both acquisition$_1$ and acquisition$_2$;
3) the median and interquartile ranges of the latency in both acquisition$_1$ and acquisition$_2$.

Statistical tests have been carried out in order to verify whether and in which learning phases significant differences in CRs rate come out between the two model populations. In particular, CRs were grouped in blocks of ten trials each and each block was compared between 1–plasticity and 3–plasticity models and between session$_1$ and session$_2$. We used the Kruskal–Wallis test to measure if there were statistical differences between CRs rates generated in the four conditions (1–plasticity session$_1$, 3–plasticity session$_1$, 1–plasticity session$_2$, and 3–plasticity session$_2$). Then, we applied a post hoc test to highlight pairwise comparisons. For all the statistical tests, the significance level p was set to 0.05.

A deeper analysis, explaining how the SNN learned to express CRs in a proper way, was carried out considering the median individual among the 3-plasticity models and the corresponding
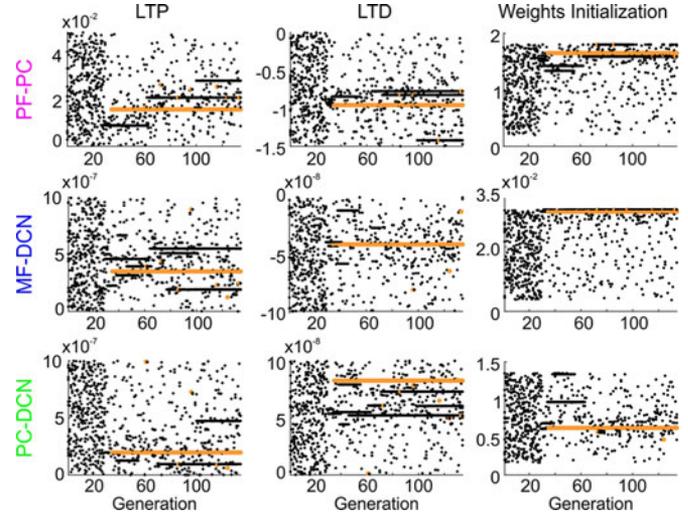

Fig. 3.   GA: Genes values along generations. For each gene (first row: PF-PC LTP_1, LTD_1, and w_{0_1}; second row: MF-DCN LTP_2, LTD_2, and w_{0_2}; third row: PC-DCN LTP_3, LTD_3, and w_{0_3}), the values explored by GA are reported as black dots (12 individuals for each generation). The genes belonging to the best models (with fitness value equal to 1) are colored in orange. On each y-axis, there are the limits of the search space for each gene (details and references in Section II). For the initialization weights (w_0), the y-axis range allowed the GA exploration bounded between the 10% and the 90% of the whole range in which the weights of those plastic connections could move during the learning protocols.
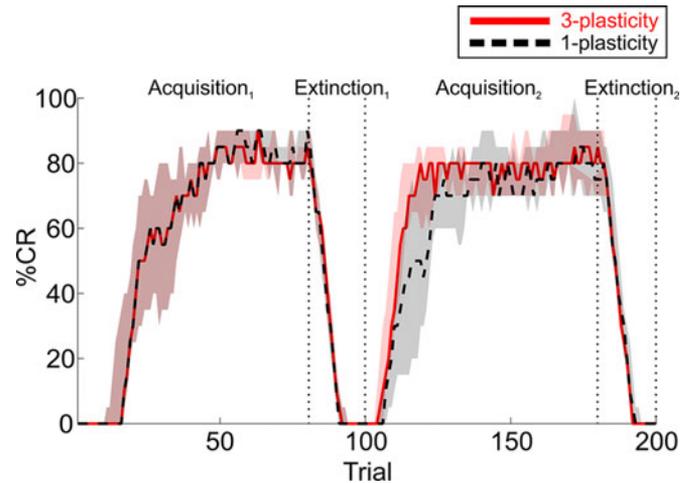

Fig. 4.   Outcomes (CR%), along the consecutive 200 trials are depicted: 80 acquisition trials and 20 of extinction trials for each of the two EBCC sessions. In red, there is reported the outcome of the median model (3–plasticity model) across all the tuned models with fitness value equal to 1, and the surrounding area represents the interquartile range. In black, there is depicted the behavioral EBCC outcome generated by the median model blocking the 2nd and 3rd plasticity mechanisms (1–plasticity model) and the surrounding area represents the interquartile ranges as well.

1-plasticity model. For both models, we inspected the evolution of spiking activity of PCs and DCNs along each of the 200 trials of EBCC simulation and along the intratrial time, computing the number of spikes of the cell populations in each time bin of 25 ms. This way, it was possible to compare the low–level differences between the 3-plasticity and 1-plasticity models, ascertaining how the firing rates of PCs and DCNs varied on account of the weights changes driven by the multiple, or single,
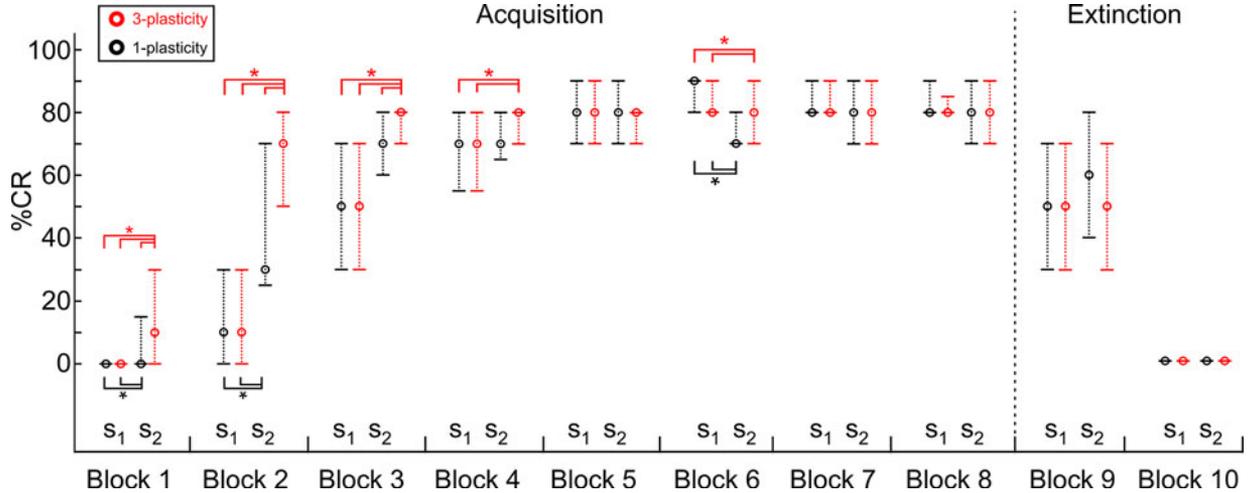
Fig. 5.   Post hoc comparison between 3-–plasticity and 1–plasticity models and between session$_1$ and session$_2$. Outcomes (CR%), along ten blocks of ten trials each are depicted as median values and interquartile ranges. For each block, the first two columns represent session$_1$ values (s$_1$), the other two columns represent session$_2$ values (s$_2$). In red, there are reported the values of 3–plasticity models (all the tuned models with fitness value equal to 1). In black, there are depicted the values of the 1–plasticity models. Asterisks indicate significant differences between groups ($p < 0.05$).

plasticities. We also verified that the firing rates did not exceed the neurophysiological values [35].

Finally, we used the parameters set of the two models' populations to carry out EBCC protocols with shorter and longer ISIs, computing the behavioral outcome of both the 3–plasticity and 1–plasticity model populations. We compared the resulting learning properties using the same indexes described above.

E. Robustness Tests

In order to verify if the GA results were reproducible and consistent, we run the optimization process five more times. Due to its intrinsic random behavior, each GA execution could identify different near optimal models driving different learning trends. We, thus, compared the behavior obtained from the optimal models coming from the six GA executions, both in session$_1$ and session$_2$.

III. RESULTS

As a first result, the GA was capable to explore the complex 9–D space of the genes, finding combinations that produced simulations reproducing EBCC learning curves similar to human data, leading the fitness to increase up to its maximum value. For the first 28 generations, the GA did not find combinations that led to a fitness greater than zero, and the genes were uniformly selected within their ranges (see Fig. 3).

Around the 30th generation, individuals with higher fitness values were identified, and the genes exploration partially focused on values in the surroundings of these individuals (Gaussian mutations) and partially explored the entire search space (Uniform mutations).

The median individual of the 3-plasticity population had the following genes: $LTP_1 = 1.6143 \times 10^{-2}$, $LTD_1 = -9.5764 \times 10^{-1}$, $w_{0_1} = 1.6499$, $LTP_2 = 3.5066 \times 10^{-7}$, $LTD_2 = -4.1308 \times 10^{-8}$, $w_{0_2} = 3.0909 \times 10^{-2}$, $LTP_3 = 1.9650 \times 10^{-7}$, $LTD_3 = 8.2685 \times 10^{-8}$, and $w_{0_3} = 6.2458 \times 10^{-1}$.

TABLE II
BEHAVIORAL OUTCOME INDEXES

	3-plasticity model		1-plasticity model	
	Acquisition$_1$	Acquisition$_2$	Acquisition$_1$	Acquisition$_2$
First trial ≥70%	31 [22 38]	14 [11 16]	31 [22 38]	20 [14 35]
CR%	70 [30 80]	80 [70 80]	70 [30 90]	70 [50 80]
Latency [ms]	45 [44 47]	47 [45 48]	45 [44 47]	45 [44 47]

The 1-plasticity models were generated keeping LTP_1 and LTD_1 constants and all the initialization weights unchanged. The behavioral outcomes of the two populations were almost identical in acquisition$_1$, extinction$_1$, and extinction$_2$, whereas they differentiated in acquisition$_2$ (see Fig. 4).

Indeed, the CR% generated by the best 3-plasticity models increased earlier than the CR% produced by the 1-plasticity models and they kept higher CR% values with a lower variability in late stable acquisition (see the red area in Fig. 4 is narrower than the grey one). The analysis of the first two indexes declared in Section II is shown in Table II and supported the hypothesis that the main differences between the two models regarded the reacquisition phase only. On the other hand, the latency values did not show significant modifications between the two sessions and between the two model populations.

The Kruskal–Wallis test, performed for each Block of ten trials, showed that there were significantly differences in the outcome of the two model populations and in the two sessions for Blocks 1–4 and Block 6. The post hoc analysis, summarized in Fig. 5, proved that the 3-plasticity model outcome in session$_2$ was significantly higher than the 1–plasticity model outcome in session$_2$ for Blocks 1–3, during the early reacquisition phase. Both the models were significantly faster with respect to session$_1$ for Blocks 1 and 2. For Blocks 5–10, no significant differences came out, except for Block 6, where
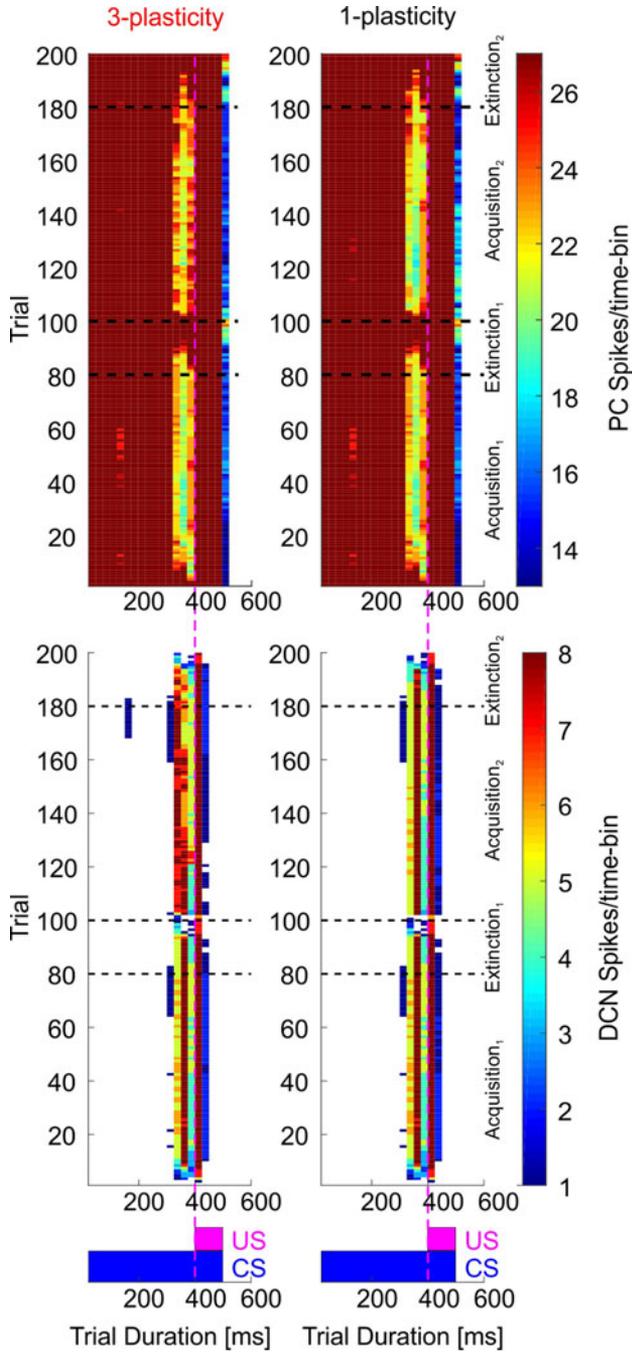
Fig. 6.   PCs and DCNs spiking patterns along all trials. The number of spikes generated within each time bin (25 ms) is reported, along trial time (600 ms) on the x-axis and along the 200 protocol trials on the y–axis. The first column reports the spiking dynamics of the 3-plasticity model (the median model across the best ones); the second column refers to the 1-plasticity model.

the outcomes in the second session were slightly lower than in the first session.

Considering the spikes patterns evolution of PCs and DCNs (see Fig. 6), there were no significant differences between the 3–plasticity model and the 1–plasticity model in the first 100 trials, whereas the PCs were more active (i.e., higher PF-PC synaptic weights) in acquisition$_2$ of the 3–plasticity than in the 1–plasticity model. Contrary to what might be thought, the

TABLE III
FIRING RATES AT EARLY ACQUISITION

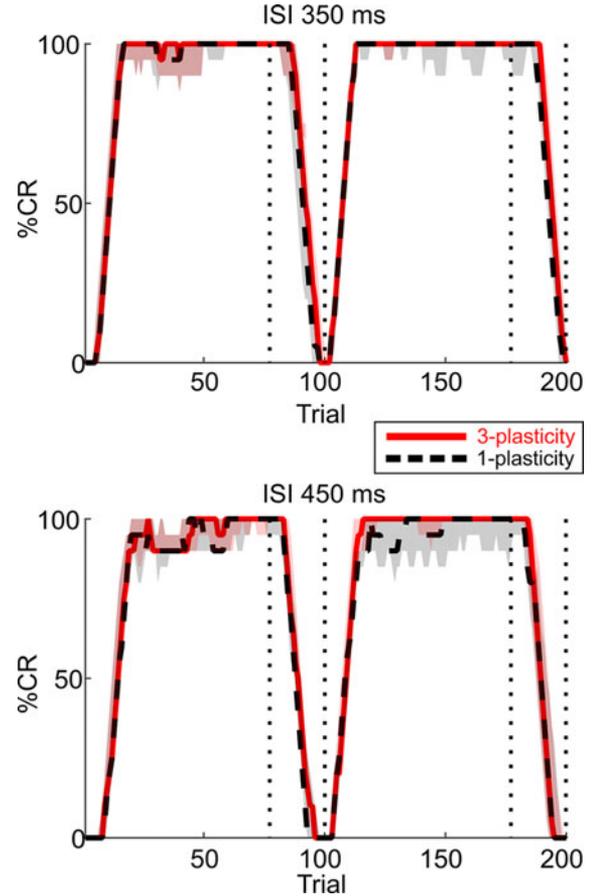|	3-plasticity model		1-plasticity model	
	20th trial	120th trial	20th trial	120th trial
PCs [Hz]	29.7 ± 10.2	29.7 ± 9.8	29.7 ± 10.2	28.2 ± 9.8
DCNs [Hz]	11.9 ± 5.7	15.1 ± 6.2	11.9 ± 5.7	14.1 ± 5.9

Fig. 7.   Model robustness: Behavioral outcomes with different EBCC protocols. As in Fig. 4, outcomes (CR%), along the consecutive 200 trials, are depicted: In red with the 3-plasticity model, and in black with 1-plasticity model. A shorter and a longer ISIs between CS and US onsets have been tested.

DCNs in acquisition$_2$ fired more with the 3-plasticity model, even though the higher PCs activity inhibited more the corresponding DCNs.

In Table III, there are reported the mean firing rates for PCs and DCNs between 300 and 400 ms from the CS onset at the 20th trial of acquisition$_1$ and of acquisition$_2$ (120th trial). The firing rates at the 20th trial were identical between the two models, whereas in early acquisition$_2$, the firing rates of PCs decreased for the 1–plasticity model only. On the other hand, the DCNs frequencies were higher for the 3–plasticity model, in spite of a higher inhibition coming from the PCs. Therefore, the firing rate values and the spike pattern analysis suggested that the better performances of the 3-plasticity model depended on the nuclear plasticity sites and their modulation capabilities.

TABLE IV
BEHAVIORAL OUTCOME INDEXES FOR DIFFERENT ISIS

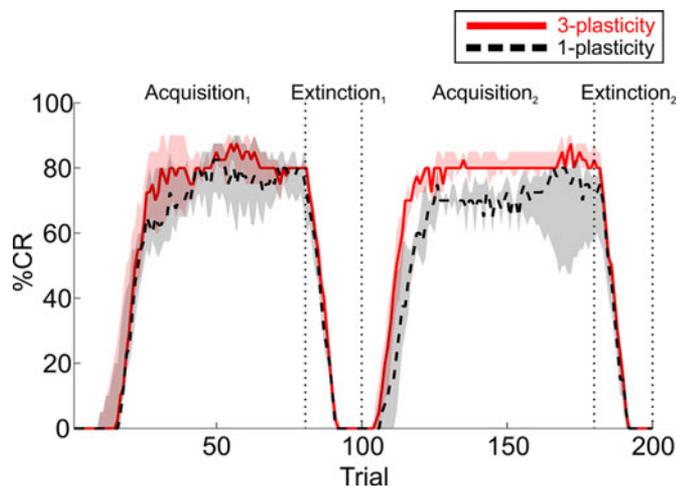| ISI 350 ms	3-plasticity model		1-plasticity model	
	Acquisition$_1$	Acquisition$_2$	Acquisition$_1$	Acquisition$_2$
First trial ≥70%	13 [11 14]	10 [9 11]	13 [11 14]	10 [9 11]
CR%	100 [90 100]	100 [100]	100 [90 100]	100 [90 100]
Latency [ms]	48 [47 49]	49 [48 49]	48 [47 49]	47 [46 48]
ISI 450 ms	3-plasticity model		1-plasticity model	
	Acquisition$_1$	Acquisition$_2$	Acquisition$_1$	Acquisition$_2$
First trial ≥70%	17 [14 17]	11 [9 12]	17 [14 17]	12 [10 12]
CR%	90 [90 100]	100 [90 100]	90 [80 100]	90 [80 100]
Latency [ms]	40 [39 41]	40 [38 44]	40 [38 41]	39 [37 40]

Fig. 8. GA robustness: Behavioral outcomes with multiple (six) GA optimization processes. As in Fig. 4, outcomes (CR%), along the consecutive 200 trials, are depicted: In red with the 3-plasticity model, and in black with 1-plasticity model.

Furthermore, the same protocol, applied to different ISIs with both the 3-plasticity and the 1-plasticity models (see Fig. 7) confirmed the robustness of the models; they were able to express learning in a physiological number of acquisition trials and to rapidly extinguish the previously acquired behavior, even if some saturation phenomenon emerged.

With different ISIs, the disparities between 3-plasticity and 1–plasticity models were less evident (see Table IV), but it is still possible to notice that the behavioral outcomes generated with the model with distributed plasticity demonstrated, taking into account the acquisition$_2$ phases, slightly faster and more stable CR%. As with ISI-baseline, the latency values did not change depending on the sessions' phases and on the number of plasticity sites embedded in the model.

Finally, the behavioral outcomes obtained from the execution of the six GAs were comparable to the one previously analyzed in details. In all the six GAs, the stopping criterion was reached in about 150 generations, and individuals with fitness equal to 1 were found in all the cases, proving the robustness and consistency of the proposed tuning approach. The outcome obtained considering all the best models of all the six GAs (see Fig. 8)

was similar to the one considered before (see Fig. 4), and the difference between the 3–plasticity model and 1–plasticity model was evident in the second acquisition phase.

IV. DISCUSSION

The studied cerebellar model exhibited realism on various aspects. The topology respected the anatomical ratios between the different groups of cells, the spiking nature of the model produced a neural activity directly comparable to neurophysiological recordings and the mean firing rates of neural population varied within acceptable ranges. Thus, the overall dynamics of the network fairly reproduced the biological behavior.

The successful results in terms of behavioral outcomes demonstrated also the high-level realism of the controller, which was able to reproduce the same responses showed in humans or animals in the same learning paradigm. For example, in both the 3-plasticity and 1-plasticity models, the CR% increase in acquisition$_2$ was more rapid than in acquisition$_1$. The same behavior was found in human subjects in multisession EBCC.

Some properties of the simulated behavior reflect directly some model parameters defined in the circuit architecture, anyway introduced based on neurophysiological knowledge at neural and network level. For example, the delay constant t_0 within the kernel of the cortical plasticity rule was crucial in determining the DCN response latencies with respect to the inhibitory action from PCs. Moreover, the search spaces for the nine genes in the GA runs were defined *a priori*, influencing the timescale of the different learning rules (LTP and LTD constants) and the ranges of firing rates of the different cell groups (initialization weights w_0), as suggested by low–level neurophysiological theories. The high-level differences in behavioral terms between the first and the second sessions or between the 1–plasticity model and the 3–plasticity model emerged from the circuit itself and our computational approach proved to be promising in directly linking specific neural properties and the human-like observed behavior.

The key element linking the spiking neural activity and the resulting motor commands is the synaptic plasticity; integrating cortical and nuclear plasticity sites at PF-PC, MF–DCN, and PC-DCN connections allowed showing up the role of the cerebellum in learning, adaptation, prediction, and memory on multiple time scales. We inferred that the action of the nuclear plasticities did not modify the timing of the CR within the trial length, since the latency values did not changed. On the other hand, the distributed plasticity modulated the DCNs activity, increasing their firing rates and improving the capability of the model to retain the behavior acquired in acquisition$_1$, in order to express CRs earlier in acquisition$_2$.

These results confirmed the physiological hypotheses on cerebellar functions [37] and were consistent with the outcome of simulations driven by analog models [19], [20]. In fact, in the idea of distributed synergistic plasticity, individual forms of plasticity are not comprehensive alone. The 3–plasticity model confirmed the hypotheses that nuclear synapses (PC-DCN and MF-DCN) are plastic on a slow time scale and store persistent memory, whereas cortical plasticity (PF-PC) could operate on

a shorter time scale, storing transient memory that could be consolidated in the nuclear plasticity sites.

It is important to emphasize that the key player in cerebellar learning was the cortical plasticity, since also the 1–plasticity model was able to generate associative responses using only the PF–PC plasticity. This finding confirms the pillar concept of the Marr–Albus–Ito motor learning theory, which entails that learning involves plasticity at the PF–PC synapses under the supervision of the CFs [6]–[8]. However, the addition of plasticity capabilities at the nuclear sites significantly impacted on the model performances during the second acquisition phase.

Even if the proposed model showed good performances and realistic behaviors, it did not include other forms of plasticity, e.g., in the granular layer [11], [38] or other neurons, e.g., the molecular layer interneurons (stellate and basket cells) [39]. Regarding the molecular interneurons, they control the simple spikes firing of the PCs by feedforward inhibition and they mediate memory consolidation processes, showed in rats during vestibuloocular reflex tasks. Future refinements of the proposed model could include this inhibitory loop to PCs, in order to verify if this additional pathway changes the memory storage capabilities of the cerebellar microcircuit in both motor and associative learning.

However, multiple learning rules for the different plasticity sites raised, from the computational point of view, the complexity of the model, increasing the number of parameters that needs to be tuned. The GA was developed and exploited as an efficient tool to tune automatically the SNN. It allowed finding the proper parameters of the model, without wasting time and resources using other techniques; in fact, typical methods like direct search or trial–and–error modulation would reveal computationally unfeasible when dealing with such complex systems and high-dimensional parameter space. Therefore, through the introduction of focused evolutionary operators and proper constraints on the parameters, the network was efficiently tuned. The final resulting solution was used for all the following tests; thus, demonstrating the generalizability of the near–optimal cerebellar microcircuit.

V. Conclusion

In this study, we compared two different SNN cerebellar models, and we challenged them to reproduce how human beings acquire and extinguish CRs during an associative motor task.

The 3-plasticity model, embedded with distributed plasticity, showed different time scales of learning and improved its performance. We validated the models robustness in learning associative responses with different ISIs, and we have shed light on acquisition, extinction, and consolidation mechanisms, associable to the different active plasticity sites.

The 3–plasticity model presents very interesting novelties, such as greater realism that resembles neurophysiological evidences and real-time characteristics, which make the model ready to be used and tested in neurorobotic applications.

Certainly, there are diverse aspects that could be improved: by increasing the number of neurons or including more realistic neuron dynamics, the model will gain in fidelity, computational power, and output resolution.

With these improvements, the here validated closed–loop cerebellar circuit can represent a promising clinical tool. Indeed, the SNN with modified parameters to reproduce cerebellar abnormalities, such as specific lesions or cellular disruption, could predict the expected and correlated behavioral outcomes. On the other hand, the evolutionary algorithm exploited in this study could be used to find the model parameters that produce an outcome fitting specific patients' misbehaviors. Thus, patient-specific models could suggest which underlying neural modifications affect certain aspects of the patients' learning performances.

References

[1] R. B. Ivry and J. V Baldo, "Is the cerebellum involved in learning and cognition?" *Curr. Opin. Neurobiol.*, vol. 2, no. 2, pp. 212–216, Apr. 1992.

[2] R. F. Thompson, "Neural mechanisms of classical conditioning in mammals," *Philos. Trans. R. Soc. Lond. Ser. B Biol. Sci.*, vol. 329, no. 1253, pp. 161–170, Aug. 1990.

[3] J. F. Medina and M. D. Mauk, "Computer simulation of cerebellar information processing," *Nature Neurosci.*, vol. 3, pp. 1205–1211, Nov. 2000.

[4] L. M. Aitkin and J. Boyd, "Acoustic input to the lateral pontine nuclei," *Hearing Res.*, vol. 1, no. 1, pp. 67–77, Oct. 1978.

[5] L. L. Sears and J. E. Steinmetz, "Dorsal accessory inferior olive activity diminishes during acquisition of the rabbit classically conditioned eyelid response," *Brain Res.*, vol. 545, nos. 1/2, pp. 114–122, Apr. 1991.

[6] D. Marr, "A theory of cerebellar cortex," *J. Physiol.*, vol. 202, no. 2, pp. 437–470, Jun. 1969.

[7] J. S. Albus, "A theory of cerebellar function," *Math. Biosci.*, vol. 10, nos. 1/2, pp. 25–61, Feb. 1971.

[8] M. Ito, "Cerebellar microcomplexes," *Int. Rev. Neurobiol.*, vol. 41, pp. 475–487, Jan. 1997.

[9] H. Jörntell and C. Hansel, "Synaptic memories upside down: Bidirectional plasticity at cerebellar parallel fiber-Purkinje cell synapses," *Neuron*, vol. 52, no. 2, pp. 227–238, Oct. 2006.

[10] C. Hansel *et al.*, "Beyond parallel fiber LTD: The diversity of synaptic and non-synaptic plasticity in the cerebellum," *Nature Neurosci.*, vol. 4, no. 5, pp. 467–475, May 2001.

[11] E. D'Angelo *et al.*, "Timing in the cerebellum: Oscillations and resonance in the granular layer," *Neuroscience*, vol. 162, no. 3, pp. 805–815, Sep. 2009.

[12] J. Monaco *et al.*, "Cerebellar theta burst stimulation dissociates memory components in eyeblink classical conditioning," *Eur. J. Neurosci.*, vol. 40, no. July, pp. 1–8, Sep. 2014.

[13] S. K. E. Koekkoek *et al.*, "Cerebellar LTD and learning-dependent timing of conditioned eyelid responses," *Science*, vol. 301, no. 5640, pp. 1736–1739, Sep. 2003.

[14] M. Schonewille *et al.*, "Purkinje cell-specific knockout of the protein phosphatase PP2B impairs potentiation and cerebellar motor learning," *Neuron*, vol. 67, no. 4, pp. 618–28, Aug. 2010.

[15] J. R. Pugh and I. M. Raman, "Potentiation of mossy fiber EPSCs in the cerebellar nuclei by NMDA receptor activation followed by postinhibitory rebound current," *Neuron*, vol. 51, no. 1, pp. 113–23, Jul. 2006.

[16] J. F. Medina and M. D. Mauk, "Simulations of cerebellar motor learning: Computational analysis of plasticity at the mossy fiber to deep nucleus synapse," *J. Neurosci.*, vol. 19, no. 16, pp. 7140–7151, Aug. 1999.

[17] E. D'Angelo *et al.*, "Distributed circuit plasticity: New clues for the cerebellar mechanisms of learning," *Cerebellum*, Aug. 2015.

[18] J. F. Medina, "Mechanisms of cerebellar learning suggested by eyelid conditioning," *Curr. Opin. Neurobiol.*, vol. 10, no. 6, pp. 717–724, Dec. 2000.

[19] J. A. Garrido *et al.*, "Distributed cerebellar plasticity implements adaptable gain control in a manipulation task: A closed-loop robotic simulation," *Front. Neural Circuits*, vol. 7, art. no. 159, Jan. 2013.

[20] C. Casellato *et al.*, "Distributed cerebellar plasticity implements generalized multiple-scale memory components in real-robot sensorimotor tasks," *Front. Comput. Neurosci.*, vol. 9, art. no. 24, Feb. 2015.

[21] R. R. Carrillo *et al.*, "A real-time spiking cerebellum model for learning robot control," *Biosystems*, vol. 94, no. 1, pp. 18–27, 2008.

[22] T. Yamazaki and J. Igarashi, "Realtime cerebellum: A large-scale spiking network model of the cerebellum that runs in realtime using a graphics processing unit," *Neural Netw.*, vol. 47, pp. 103–111, Nov. 2013.

[23] C. Casellato *et al.* "Adaptive robotic control driven by a versatile spiking cerebellar network," *PLoS One*, vol. 9, no. 11, p. e112265, Nov. 2014.

[24] K. D. Carlson *et al.*, "An efficient automated parameter tuning framework for spiking neural networks," *Front. Neurosci.*, vol. 8, art. no. 10, Jan. 2014.

[25] S. Voß, "Meta-heuristics: The state of the art," in *Local Search for Planning and Scheduling*, vol. 2148. Berlin, Germany: Springer, 2001, pp. 1–23.

[26] E. Ros *et al.*, "Event-driven simulation scheme for spiking neural networks using lookup tables to characterize neuronal dynamics," *Neural Comput.*, vol. 18, no. 12, pp. 2959–2993, Dec. 2006.

[27] I. Herreros and P. F. M. J. Verschure, "Nucleo-olivary inhibition balances the interaction between the reactive and adaptive layers in motor control," *Neural Netw.*, vol. 47, pp. 64–71, Nov. 2013.

[28] M. Gerwig *et al.*, "Timing of conditioned eyeblink responses is impaired in cerebellar patients," *J. Neurosci.*, vol. 25, no. 15, pp. 3919–3931, Apr. 2005.

[29] G. Hesslow *et al.*, "Classical conditioning of motor responses: What is the learning mechanism," *Neural Netw.*, vol. 47, pp. 81–87, Nov. 2013.

[30] S. N. Chettih *et al.*, "Adaptive timing of motor output in the mouse: The role of movement oscillations in eyelid conditioning," *Front. Integr. Neurosci.*, vol. 5, art. no. 72, Jan. 2011.

[31] N. R. Luque *et al.*, "Cerebellarlike corrective model inference engine for manipulation tasks," *IEEE Trans. Syst. Man, Cybern. B, Cybern.*, vol. 41, no. 5, pp. 1299–1312, Oct. 2011.

[32] A. Antonietti *et al.*, "Spiking cerebellar model with multiple plasticity sites reproduces eye blinking classical conditioning," in *Proc. IEEE/EMBS 7th Int. Conf. Neural Eng.*, 2015, pp. 296–299.

[33] N. R. Luque *et al.*, "Adaptive cerebellar spiking model embedded in the control loop: Context switching and robustness against noise," *Int. J. Neural Syst.*, vol. 21, no. 5, pp. 385–401, Oct. 2011.

[34] R. R. Carrillo *et al.*, "Event-driven simulation of neural population synchronization facilitated by electrical coupling," *Biosystems.*, vol. 87, nos. 2/3, pp. 275–280, Feb. 2007.

[35] J. F. Medina and K. S. Garcia, "Timing mechanisms in the cerebellum: Testing predictions of a large-scale computer simulation," *J. Neurosci.*, vol. 20, no. 14, pp. 5516–5525, 2000.

[36] D. E. Goldberg and K. Deb, "A comparative analysis of selection schemes used in genetic algorithms," *Found. Genet. Algorithms*, vol. 1, pp. 69–93, 1991.

[37] L. Mapelli *et al.* "Integrated plasticity at inhibitory and excitatory synapses in the cerebellar circuit," *Front. Cell. Neurosci.*, vol. 9, pp. 1–17, May 2015.

[38] S. Solinas *et al.*, "A realistic large-scale model of the cerebellum granular layer predicts circuit spatio-temporal filtering properties," *Front. Cell. Neurosci.*, vol. 4, art. no. 12, Jan. 2010.

[39] P. Wulff *et al.*, "Synaptic inhibition of Purkinje cells mediates consolidation of vestibulo-cerebellar motor learning," *Nature Neurosci.*, vol. 12, no. 8, pp. 1042–1049, Aug. 2009.

Authors' photographs and biographies not available at the time of publication.